Magnetoelastic Coupling and Symmetry Breaking in the Frustrated Antiferromagnet α-$NaMnO_2$

Maud Giot,[1,2] Laurent C. Chapon,[2] John Androulakis,[1] Mark A. Green,[3,4] Paolo G. Radaelli,[2] and Alexandros Lappas[1,*]

[1]*Institute of Electronic Structure and Laser, Foundation for Research and Technology - Hellas, Vassilika Vouton, 71110 Heraklion, Greece*

[2]*ISIS, Science and Technology Facilities Council, Rutherford Appleton Laboratory, Chilton-Didcot, OX11 0QX, Oxfordshire, United Kingdom*

[3]*NIST Center for Neutron Research, 100 Bureau Drive, Gaithersburg, Maryland 20899-8562, USA*

[4]*Department of Materials Science and Engineering, University of Maryland, College Park, Maryland 20742-2115, USA*

(Received 1 August 2007; published 14 December 2007)

The magnetic and crystal structures of the α-$NaMnO_2$ have been determined by high-resolution neutron powder diffraction. The system maps out a frustrated triangular spin lattice with anisotropic interactions that displays two-dimensional spin correlations below 200 K. Magnetic frustration is lifted through magneto-elastic coupling, evidenced by strong anisotropic broadening of the diffraction profiles at high temperature and ultimately by a structural phase transition at 45 K. In this low-temperature regime a three-dimensional antiferromagnetic state is observed with a propagation vector $\mathbf{k} = (\frac{1}{2}, \frac{1}{2}, 0)$.

DOI: 10.1103/PhysRevLett.99.247211 PACS numbers: 75.25.+z, 61.12.Ld, 75.30.Kz, 75.80.+q

Triangular magnetic lattices with antiferromagnetic (AFM) nearest-neighbor interactions have been the subject of a number of studies because various exotic ground states are predicted including the transition to a spin liquid [1,2]. The triangular lattice with anisotropic exchange interactions, i.e., J_1 along one of the triangle directions and J_2 along the other two [$J_1 \neq J_2$, see Fig. 1(a)], has been of particular interest for theoreticians since the early 1970s [3], along the lines of the famous work of Onsager on the square lattice [4]. The predicted magnetic phase diagram as a function of J_2/J_1, for example, in a spin-$\frac{1}{2}$ lattice, is extremely rich [5,6]: Néel or dimerized ground states are stabilized for large J_2/J_1 ratios (>1). For lower J_2/J_1, a spiral order is expected in the Heisenberg limit but there is still controversy for small J_2/J_1 (<0.2), in the so-called *zigzag* or weakly coupled chains model. In the latter, AFM correlations should be established along chains (J_1), but interchain coupling (J_2) is frustrated since the magnetic energy is invariant by flipping any of the AFM chains in the lattice. A few experimental realizations of this model have been reported, whereas *larger spin-size* lattices remain rare systems to study. A recent neutron work on the $S = 1/2$ Cs_2CuCl_4 triangular Heisenberg antiferromagnet (with $J_2/J_1 = 0.175$) has revealed three-dimensional (3D) magnetic order with cycloidal modulation [7]. When a magnetic field is applied perpendicular to the chains, the AFM order is suppressed and magnetic excitations are those of a $S = 1/2$ one-dimensional (1D) Heisenberg antiferromagnet, suggesting decoupled AFM chains [8,9].

Triangular lattices are also found in many compounds with the general formula α-AMO_2 (A = Li, Na, K, Ag, M = transition-metal). In particular, the α-$NaFeO_2$ analogues are layered compounds where magnetic M ions are organized in a triangular lattice topology [10]. Edge-sharing MO_6 octahedra form layers separated by hexagonal nets of A cations. These two-dimensional (2D) systems, well known for their applications in rechargeable batteries [11], have also attracted considerable interest for their fundamental physics [12–14]. If M is Jahn-Teller active, the elongated bonds point in the same direction (ferro-orbital ordering), leading to a crystal structure that maps out a triangular spin lattice with anisotropic interactions. However, the best-known member of this group—α-$NaNiO_2$—is not frustrated, since the magnetic coupling in the plane is ferromagnetic (FM; J_1, $J_2 > 0$) [15].

Here we show that unlike any other member of the series, α-$NaMnO_2$ realizes a zigzag ($S = 2$) chain model (J_1, $J_2 < 0$, J_2/J_1 small) due to a dominant direct-exchange interaction perpendicular to the ferro-orbital or-

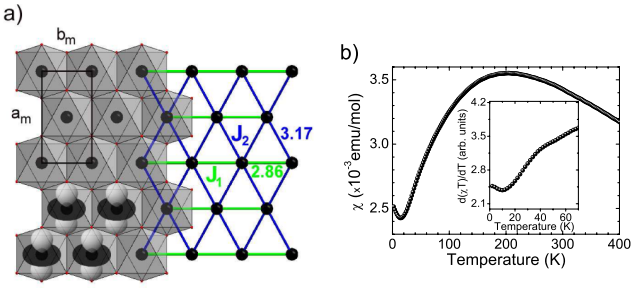

FIG. 1 (color online). α-$NaMnO_2$: (a) crystal structure in the $a_m b_m$ plane at room temperature. Mn and O atoms are represented as large black and small red spheres, respectively. MnO_6 octahedra are shown in transparent gray together with $d_{3r^2-z^2}$ orbitals. The green and blue lines show inequivalent (J_1, J_2) magnetic interactions along b_m and $[110]_m$ (subscript m for monoclinic). (b) Temperature evolution of the magnetic susceptibility, χ ($H = 1$ T; zero-field cooled data). Inset: the derivative of χT vs T.

dering direction. Neutron powder diffraction (NPD) shows that the existence of 2D static spin correlations within the triangular planes is followed, despite the frustration, by 3D long-range magnetic order below $T_N = 45$ K. Our crystallographic analysis reveals that the degeneracy of the ground state is lifted by magneto-elastic coupling, evidenced by anisotropic broadening of the Bragg peaks in the 2D regime and by a structural transition to a triclinic cell below T_N. In both magnetic phases, the moment direction, fixed by the crystalline field, points towards the apical oxygens, indicating that the system possesses magnetic easy-axis anisotropy.

Polycrystalline samples of α-$NaMnO_2$ were prepared according to earlier report [16]. NPD data were collected at NIST on the BT1 diffractometer ($\lambda = 2.0787$ Å) at several temperatures between 4 K and 500 K. Rietveld analysis was carried out using the FULLPROF suite [17]. Magnetic susceptibility data were obtained at the Well Fund Laboratory at ISIS using a commercial SQUID magnetometer $2 \leq T \leq 400$ K ($H = 1$ T). During the measurements, the sample environment was carefully controlled as the material hydrolyzes under ambient conditions.

The room temperature (RT) monoclinic (m) structure of α-$NaMnO_2$ refined from our NPD data is in agreement with that determined earlier by single crystal x-ray diffraction [18]. The Mn^{3+} ions occupy the $2a$ site, (0,0,0), octahedrally coordinated by oxygens in the $4i$ site, [0.2936(2), 0, 0.7957(2)]. $Mn^{3+}O_6$ octahedra share edges to form MnO_2 layers in the $a_m b_m$ plane, as shown in Fig. 1(a). All octahedra around Jahn-Teller active Mn^{3+} ions (high spin, $3d^4$ electronic configuration) are axially elongated along the same direction in the $a_m c_m$ plane, corresponding to ferro-orbital ordering of the $d_{3r^2-z^2}$ orbitals [Fig. 1(a)]. The cooperative distortion results in inequivalent magnetic exchange integrals within the triangular Mn lattice, namely, of J_1 along the b_m axis and J_2 along the other two directions. The magnetic topology maps out a triangular lattice with anisotropic interactions, which can also be described as a square lattice (J_2) with a single diagonal interaction (J_1) [5]. All the Mn-O-Mn superexchange interactions are weak due to the nearly 90° angles and predominantly FM [12,19,20]. However, unlike the case of α-$NaNiO_2$, the half-filled t_{2g} Mn^{3+} orbitals along the short Mn-Mn distance of edge-sharing octahedra promote strong AFM direct-exchange interactions, leading to interchain frustration (*vide supra*). Magnetic interactions between adjacent MnO_2 planes, interleaved by a layer of Na ions positioned at the $2d$ site, ($\frac{1}{2}$, 0, $\frac{1}{2}$), are weaker as compared to the in-plane interactions.

Magnetic susceptibility [Fig. 1(b)] shows deviation from the Curie-Weiss behavior in the entire T range. The broad maximum around 200 K is typical of low-dimensional AFM interactions [21]. The paramagnetic (PM) approximation is not valid as neutron diffraction finds (*vide infra*) significant short-range 2D static spin correlations that extend to the higher temperature regime. Upon cooling, the susceptibility decreases continuously, however, with a small anomaly at ~40 K, as witnessed in the derivative of χT versus T [inset of Fig. 1(b)]. The pronounced drop of χ below 40 K indicates the onset of enhanced AFM correlations and 3D magnetic ordering as it will be explained below. Analysis of the α-$NaMnO_2$ susceptibility (at $T > 40$ K), based on finite temperature Lanzos method calculations on various size spin clusters, supports the picture of stronger exchange along the J_1 (~65 K) bond direction, with $J_2/J_1 \sim 0.44$ [22].

NPD experiments below RT also show two magnetic regimes. Below 200 K, broad asymmetric features are observed around the $(\frac{h}{2}, \frac{k}{2}, 0)_m$ Bragg positions, the strongest being at $(\frac{1}{2}, \frac{1}{2}, 0)_m$ (inset of Fig. 2). The asymmetry of the signal with a tail on the high-Q side is typical of scattering from 2D lattices, as described initially by Warren [23]. We have also considered a scenario where the AFM chain formation along b_m may give rise to diffuse scattering with one-dimensional features. In this case ones expects diffuse scattering with a steplike form [24,25] to be resolved at the $(0, \frac{1}{2}, 0)_m$ Bragg position, corresponding to a Q vector of 1.10 $Å^{-1}$. This is in contrast to the diffuse peak centered at the $Q = 1.25$ $Å^{-1}$ in the present experiments. The intensity of this signal increases on cooling to ~45 K, where sharp magnetic Bragg peaks appear. These can be indexed with a propagation vector $\mathbf{k} = (\frac{1}{2}, \frac{1}{2}, 0)_m$ in the monoclinic cell. The Warren scattering decreases rapidly

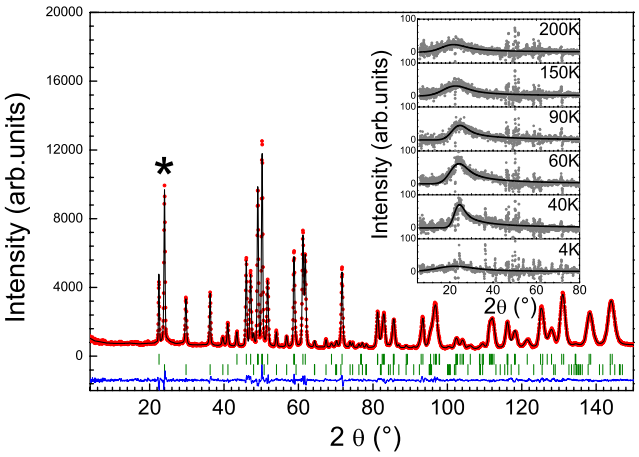

FIG. 2 (color online). Rietveld refinement of neutron powder diffraction data obtained at 4 K for α-$NaMnO_2$ in the triclinic cell. The red points and black line represent the data and calculated profile, respectively. The blue line at the bottom is the difference between observed and calculated patterns. Tick marks show the position of Bragg peaks for the nuclear (top line) and magnetic phases (bottom line). The * symbol marks the position of the $(0, \frac{1}{2}, 0)_t$ magnetic Bragg peak, indexed in the triclinic cell (subscript t). Inset: temperature evolution of the Warren scattering (gray symbols); black lines are fit to the data (see text for details).

below T_N and is found to coexist with the 3D magnetically ordered phase but is not totally suppressed at 4 K.

The low-temperature magnetic structure has been determined by Rietveld refinement using solutions derived from representation analysis. A single spin configuration was found to reproduce the data, with very good agreement factors [$\chi^2 = 3.82$, $R_{\text{Bragg}} = 1.56\%$, $R(F^2) = 1.19\%$, $R_{\text{magn}} = 5.63\%$]. At 4 K, the components of the moment are $-1.79(6)\mu_B$ and $1.71(6)\mu_B$ along the x_m and z_m crystallographic directions, respectively. The spins point along the direction of the $d_{3r^2-z^2}$ orbitals, in support of an easy-axis anisotropy at the Mn^{3+} site. The 4 K value of the staggered moment, $2.92(2)\mu_B/Mn^{3+}$, is considerably reduced with respect to the saturated $4\mu_B$ expected for $S = 2$. The spin arrangement (Fig. 3) consists of AFM chains running along the monoclinic b_m axis. In the $a_m b_m$ plane, the chains are stacked ferromagnetically along the $[1\bar{1}0]_m$ direction and antiferromagnetically along $[110]_m$. Coupling between adjacent MnO_2 layers along the c_m direction is FM. Rietveld analysis of all data shows that the magnetic arrangement and the orientation of the moments do not depend on temperature below $T_N = 45$ K. The evolution of the staggered moment is shown in Fig. 4(a). On warming to 45 K, the magnetic Bragg signal is gradually transferred into 2D Warren scattering. The position of the Warren scattering $(\frac{h}{2}, \frac{k}{2})_m$ suggests the progressive loss of long-range correlations along the c axis, compatible with the much weaker exchange interaction along this direction. The lack of reorientation of the Mn-spin direction within the planes, in both 2D and 3D magnetic regimes, may suggest that the system rests in the Ising limit. Future inelastic neutron scattering experiments and theoretical calculations will be invaluable in this respect.

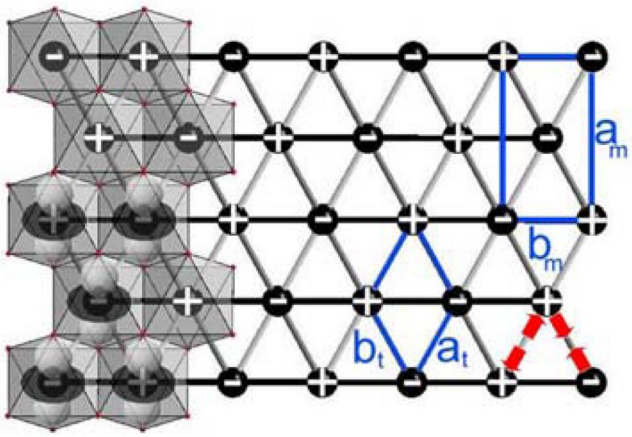

FIG. 3 (color online). Schematic representation of the magnetic order in the ab plane for α-$NaMnO_2$. The + and − signs indicate the direction of the magnetic moments along the $d_{3r^2-z^2}$ orbital shown in gray. The blue lines mark the high-temperature monoclinic (a_m, b_m) and low-temperature triclinic (a_t, b_t) unit cells. Red arrows show the strain directions.

Furthermore, the pure magnetic Warren scattering has been extracted by subtracting the calculated neutron diffraction pattern from a constant background. The signal (inset Fig. 2) has been modeled assuming that the configuration and orientation of spins in the triangular layer is the same as that of the 3D magnetic structure, but with a totally incoherent stacking of magnetic layers along the c direction. The powder-averaged magnetic intensity of the $(\frac{1}{2}, \frac{1}{2})_m$ magnetic peak has been calculated assuming a Gaussian spin-spin correlation function [26]. The value of the 2D-ordered moment is $4.2(4)\mu_B$ at ~50 K where the Warren scattering is most intense, indicating a fully saturated moment. This is consistent with the $\chi(T)$, where only a weak anomaly is observed at the crossover from 2D to 3D magnetic regimes. The correlation length [Fig. 4(b)] is only $\xi \sim 30$ Å at this temperature, indicating that in-plane AFM correlations are relatively short range in the 2D regime. The correlation length decreases on warming and levels out to $\xi \sim 10$ Å. Above 200 K the Warren scattering becomes too weak and diffuse to be observed through this powder measurement. However, the 2D spin correlations can prevail at least up to 400 K as suggested by the deviation of the magnetic susceptibility from the PM behavior.

The 3D and 2D magnetic arrangements derived from NPD indicate the existence of strongly coupled AFM chains along the b_m axis. However, irrespective of the value or sign of J_2, this magnetic configuration leads to a cancellation of the interchain exchange in the mean field limit. The observation of long-range magnetic order therefore points towards a mechanism that lifts the degeneracy

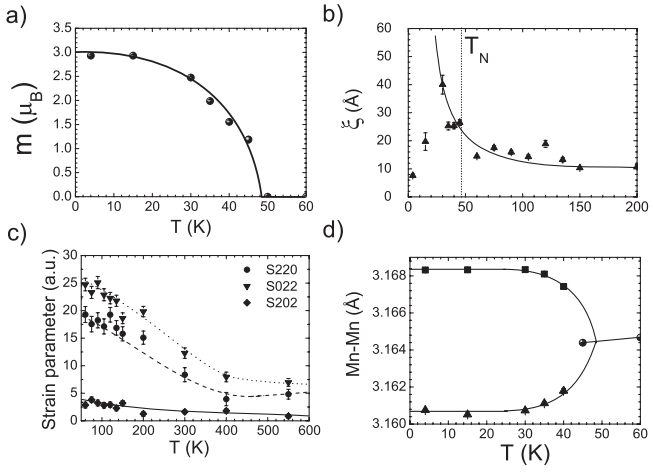

FIG. 4. Variation of magnetic and structural parameters vs temperature for α-$NaMnO_2$. (a) Mn magnetic moment in the 3D ordered phase. (b) Correlation length of the magnetic domains in the 2D magnetic phase. (c) Selected microstrain coefficients in the 2D magnetic regime (see text for details). (d) Mn-Mn interatomic distances along the a (square symbol) and b axis (triangles) in the triclinic cell; the filled circles show the distances in the monoclinic phase.

of the ground state. We were able to determine this mechanism directly from the thorough analysis of the crystal structure. Our refinements indicate that 2D and 3D magnetic order in this system are correlated to the onset of anisotropic strains. At 500 K, the crystallographic model of Jansen and Hoppe [18] fits the data perfectly using a standard isotropic description of the peak profile. However, at $T \leq 300$ K we notice a substantial broadening of h, k, l Bragg reflections with nonzero k that increases as the temperature is lowered. A full profile analysis including anisotropic microstrain parameters [27] accounts very well for the observed diffraction pattern. In this formalism, the Gaussian widths of the Bragg peaks are modeled by a fourth-term expansion, with respect to the Miller indices, h, k, l, that depends on a set of parameters S_{hkl}. All parameters that contain a k component and nonzero h or l are larger and increase upon cooling. Selected parameters are shown in Fig. 4(c). We note that the value of the S_{202} parameter remains small in the entire T range, whereas the S_{022}, S_{220} are much larger and increase below 300 K. This picture becomes clearer below T_N, where, in addition to a further increase of the strain parameters (not shown), the observed reflections at low-Q are slightly shifted with respect to their calculated positions in the monoclinic cell.

These offsets cannot be taken into account by a small incommensurability of the magnetic structure but require a lowering of the crystal symmetry at low temperature. The best fit to the data below T_N is obtained with a triclinic unit cell (symmetry $P\,\bar{1}$) and a much smaller anisotropic broadening (Fig. 2). The triclinic cell (subscript t) is related to the monoclinic cell (subscript m) by: $a_t = \frac{1}{2}(a_m - b_m)$, $b_t = \frac{1}{2}(a_m + b_m)$ (Fig. 3). The refinement of the 4 K data set (Fig. 2) leads to the following cell parameters: $a_t = 3.16773(7)$ Å, $b_t = 3.16046(7)$ Å, $c_t = 5.78217(6)$ Å, $\alpha_t = 110.465(2)°$, $\beta_t = 110.415(2)°$, $\gamma_t = 53.6173(8)°$. The magnetic propagation vector becomes $\mathbf{k} = (0, \frac{1}{2}, 0)_t$ in the triclinic setting [with $m = 2.94(2)\mu_B$, $\phi = 25(1)°$, $\theta = -56.1(8)°$ in a spherical coordination system]. This lowering of symmetry leads to better agreement factors, especially for the magnetic structure [$\chi^2 = 2.75$, $R_{\text{Bragg}} = 2.10\%$, $R(F^2) = 1.10\%$, $R_{\text{magn}} = 4.00\%$]. The structural distortion (point groups $2/m \rightarrow \bar{1}$), involving the ϵ_{xy} and ϵ_{yz} components of the strain tensor, is consistent with the anisotropic broadening of the peak profiles observed in the 2D regime. This phase transition corresponds to the *lengthening* of one of the in-plane Mn-Mn interatomic distances (along J_2) and the *contraction* of the other one [Fig. 4(d)]. Therefore, it is directly coupled to the different magnetic interactions along these directions. The magnetic frustration is clearly lifted by such a distortion, suggesting that the elastic energy cost for distorting the structure (usually quadratic in the displacements) is compensated by the magneto-elastic energy gain (linear in the displacements).

In summary, our neutron diffraction and magnetization data demonstrate that α-$NaMnO_2$ is an experimental realization of a triangular antiferromagnet with anisotropic exchange interactions (J_1, $J_2 < 0$) in the weakly coupled chain limit. The interchain magnetic frustration is lifted by magneto-elastic coupling that results in a small but observable structural distortion intimately related to the long-range ordered antiferromagnetic ground state.

We acknowledge partial support from the European Commission (''Construction of New Infrastructures'', Contract No. 011723).

*Corresponding author.
lappas@iesl.forth.gr

[1] G. Wannier, Phys. Rev. **79**, 357 (1950).
[2] T. P. Eggarter, Phys. Rev. B **12**, 1933 (1975).
[3] Y. Takana and N. Uryû, J. Phys. Soc. Jpn. **44**, 1091 (1978).
[4] L. Onsager, Phys. Rev. **65**, 117 (1944).
[5] Z. Weihong *et al.*, Phys. Rev. B **59**, 14 367 (1999).
[6] S. R. White and I. Affleck, Phys. Rev. B **54**, 9862 (1996).
[7] R. Coldea *et al.*, J. Phys. Condens. Matter **8**, 7473 (1996).
[8] R. Coldea *et al.*, Phys. Rev. Lett. **79**, 151 (1997).
[9] M. Q. Weng *et al.*, Phys. Rev. B **74**, 012407 (2006).
[10] T. A. Hewston and B. L. Chamberland, J. Phys. Chem. Solids **48**, 97 (1987).
[11] M. Winter *et al.*, Adv. Mater. **10**, 725 (1998).
[12] M. V. Mostovoy and D. I. Khomskii, Phys. Rev. Lett. **89**, 227203 (2002).
[13] C. A. Marianetti *et al.*, Phys. Rev. B **63**, 224304 (2001).
[14] K. Takada *et al.*, Nature (London) **422**, 53 (2003).
[15] C. Darie *et al.*, Eur. Phys. J. B **43**, 159 (2005).
[16] J.-P. Parant *et al.*, J. Solid State Chem. **3**, 1 (1971).
[17] J. Rodríguez-Carvajal, Physica (Amsterdam) **192B**, 55 (1993).
[18] M. Jansen and R. Hoppe, Z. Anorg. Allg. Chem. **399**, 163 (1973).
[19] J. Goodenough *et al.*, Phys. Rev. **124**, 373 (1961).
[20] J. E. Greedan *et al.*, J. Solid State Chem. **128**, 209 (1997).
[21] O. Kahn, *Molecular Magnetism* (Wiley-VCH, New York, 1993).
[22] A. Zorko, S. El Shawish, D. Arcon, Z. Jaglicic, A. Lappas, H. van Tol, and L. C. Brunel (to be published).
[23] B. E. Warren, Phys. Rev. **59**, 693 (1941).
[24] C. E. Chen *et al.*, Phys. Rev. B **25**, 2472 (1982).
[25] P. Lone *et al.*, J. Magn. Magn. Mater. **284**, 92 (2004).
[26] S. Y. Wu *et al.*, Phys. Rev. B **54**, 10 019 (1996).
[27] P. W. Stephens, J. Appl. Crystallogr. **32**, 281 (1999).